Available online at www.sciencedirect.com

ScienceDirect

Geochimica et Cosmochimica Acta 126 (2014) 541–554

Geochimica et Cosmochimica Acta

www.elsevier.com/locate/gca

Clumped isotope thermometry of cryogenic cave carbonates

Tobias Kluge [a,*,1], Hagit P. Affek [a], Yi Ge Zhang [a], Yuri Dublyansky [b], Christoph Spötl [b], Adrian Immenhauser [c], Detlev K. Richter [c]

[a] Department of Geology and Geophysics, Yale University, 210 Whitney Avenue, New Haven, CT 06511, USA
[b] Institut für Geologie, Universität Innsbruck, Innrain 52, 6020 Innsbruck, Germany
[c] Institut für Geologie, Mineralogie und Geophysik, Ruhr-Universität Bochum, Universitätsstraße 150, 44801 Bochum, Germany

Received 13 December 2012; accepted in revised form 8 November 2013; available online 23 November 2013

Abstract

Freezing of cave pool water that is increasingly oversaturated with dissolved carbonate leads to precipitation of a very specific type of speleothems known as cryogenic cave carbonates (CCC). At present, two different environments for their formation have been proposed, based on their characteristic carbon and oxygen isotope ratios. Rapidly freezing thin water films result in the fast precipitation of fine-grained carbonate powder (CCC_{fine}). This leads to rapid physicochemical changes including CO_2 degassing and $CaCO_3$ precipitation, resulting in significantly ^{13}C-enriched carbonates. Alternatively, slow carbonate precipitation in ice-covered cave pools results in coarse crystalline CCC (CCC_{coarse}) yielding strongly ^{18}O-depleted carbonate. This is due to the formation of relatively ^{18}O-enriched ice causing the gradual depletion of ^{18}O in the water from which the CCC precipitates.

Cryogenic carbonates from Central European caves were found to have been formed primarily during the last glacial period, specifically during times of permafrost thawing, based on the oxygen isotope ratios and U–Th dating. Information about the precise conditions of CCC_{coarse} formation, i.e. whether these crystals formed under equilibrium or disequilibrium conditions with the parent fluid, however, is lacking. An improved understanding of CCC_{coarse} formation will increase the predictive value of this paleo-permafrost archive.

Here we apply clumped isotopes to investigate the formation conditions of cryogenic carbonates using well-studied CCC_{coarse} from five different cave systems in western Germany. Carbonate clumped isotope measurements yielded apparent temperatures between 3 and 18 °C and thus exhibit clear evidence of isotopic disequilibrium. Although the very negative carbonate $\delta^{18}O$ values can only be explained by gradual freezing of pool water accompanied by preferential incorporation of ^{18}O into the ice, clumped isotope-derived temperatures significantly above expected freezing temperatures indicate incomplete isotopic equilibration during precipitation of CCC.

1. INTRODUCTION

Carbon and oxygen isotopes in speleothem calcite are used to reconstruct climatic and environmental conditions during speleothem growth (e.g., McDermott, 2004; Fairchild et al., 2006; Fairchild and Baker, 2012). Almost all paleoclimate studies use stalagmites or flowstones, namely speleothems precipitated from groundwater that is super-saturated with respect to calcite. Growth of stalagmites and flowstones, however, may stop if the water supply vanishes, for example, as a result of a long-lasting drought or the development of permafrost above the cave. Recently, a new type of speleothems termed cryogenic cave carbonates (CCC; Žák et al., 2004) has drawn increasing attention since it might close a data gap that exists for glacial periods, when permafrost prevents 'normal' speleothem growth

* Corresponding author. Tel.: + 49 6221 54 6350; fax: + 49 6221 54 6405.
E-mail addresses: t.kluge@imperial.ac.uk, tobias.kluge@iup.uni-heidelberg.de (T. Kluge).
[1] Present address: Institut für Umweltphysik, Universität Heidelberg, Heidelberg, Im Neuenheimer Feld 229, 69120 Heidelberg, Germany.

0016-7037/$ - see front matter © 2013 Elsevier Ltd. All rights reserved.
http://dx.doi.org/10.1016/j.gca.2013.11.011

(e.g., Richter et al., 2010; Žák et al., 2012; Luetscher et al., 2013).

CCC were first described by Kunsky (1939) who related their origin to freezing cave water. They can be subdivided into two groups based on the crystal sizes and morphology: fine-crystalline CCC (CCC_{fine}) and coarse-grained carbonate precipitates (CCC_{coarse}). Although a specific type of CCC (CCC_{fine}) forms today in some ice caves (e.g., Eisriesenwelt; Spötl, 2008 or Caverne de l'Ours; Lacelle et al., 2009), permafrost conditions conducive to the formation of CCC were much more widespread during glacial periods (Van Vliet-Lanoë, 1989; Renssen and Vandenberghe, 2003). The low temperatures led to permafrost development in the catchment area of the cave, inhibiting groundwater recharge and therefore largely preventing the growth of "normal" vadose speleothems such as stalagmites. Instead, freezing of water in such cave environments increases the saturation state with respect to calcite and eventually gives rise to the precipitation of CCC. Therefore, the presence of CCC_{coarse} has been suggested as an indicator for past permafrost occurrence and variability (Žák et al., 2012). CCC_{fine} can form in ice caves that are located in permafrost-free regions (e.g., Spötl, 2008) and, thus, are not regarded as reliable indicators of the presence of paleopermafrost. CCC occurrence in mid-latitudes is related to periods of large climatic variations within glacial stages, either to the onset of permafrost conditions that led to the freezing of cave pools (Richter et al., 2010, 2011) or to partial melting of the permafrost in the top part of the vadose zone allowing water to reach the cave chambers that still remained at sub-zero temperatures (Pielsticker, 2000; Žák et al., 2012). U–Th ages confirm this connection and indicate that CCC_{coarse} preferentially formed during glacial periods (Žák et al., 2012).

CCC grains, which consist of loose crystals of varying morphology and size, are generally characterized by a trend towards ^{13}C-enrichment and ^{18}O-depletion compared to stalagmites formed from similar cave drip waters (Žák et al., 2008). The ^{18}O depletion is related to preferential partitioning of ^{18}O into the forming ice (O'Neil, 1968; Lehmann and Siegenthaler, 1991), leaving ^{18}O-depleted water in which the crystals grow. ^{13}C enrichment is caused by Rayleigh fractionation of the dissolved inorganic carbon (DIC) whereby light ^{12}C partitions into evolving CO_2, leaving the remaining HCO_3^- enriched in ^{13}C. These signals are recorded in the precipitating CCC minerals, resulting in $\delta^{18}O$ values as negative as $-24‰$ and $\delta^{13}C$ values up to $+18‰$ (Žák et al., 2004, 2008, 2012; Richter et al., 2010, 2011).

Different freezing mechanisms and precipitation rates have been suggested to cause the formation of the two distinct groups of CCC (Žák et al., 2008):

(a) Fine-crystalline carbonate powder (<50 μm, CCC_{fine}) is thought to have formed in thin water films. Fast freezing causes strong isotopic disequilibrium effects related to rapid reaction rates, fast CO_2 degassing, and limited isotopic equilibration (Clark and Lauriol, 1992) resulting in very positive $\delta^{13}C$ (up to $+18‰$) and $\delta^{18}O$ values (up to $-2‰$; Lacelle, 2007; Spötl, 2008; Žák et al., 2008).

(b) Larger crystals (mm to cm size, CCC_{coarse}) are thought to have formed in slow gradually freezing pool water (Žák et al., 2008), where super-saturation is created through ion rejection from the forming ice. This leads to slow mineral growth and strongly ^{18}O-depleted $CaCO_3$ ($\delta^{18}O$: $-24‰$ to $-10‰$; Žák et al., 2012), but it is unknown whether CCC_{coarse} grows at isotopic equilibrium.

Carbonate clumped isotope analyses (reported as Δ_{47}) are typically used to determine the formation temperature of carbonate minerals (Eiler, 2007, 2011; Affek, 2012). However, the sensitivity of Δ_{47} to degassing makes it valuable also for the investigation of isotopic disequilibrium (Guo, 2008; Kluge and Affek, 2012). The carbonate clumped isotope thermometry is based on the temperature-dependent overabundance of ^{13}C–^{18}O bonds in the crystal lattice compared to a stochastic distribution.

Depending on the conditions during carbonate formation, a varying degree of disequilibrium has been observed in clumped and oxygen isotopes of 'normal' speleothems (e.g., Mickler et al., 2006; Tremaine et al., 2011) complicating their interpretation. For stalagmites, an offset in $\delta^{18}O$ of about $1‰$ with respect to the isotopic equilibrium value is typically observed (McDermott et al., 2011) with a corresponding large offset in clumped isotopes (Affek et al., 2008; Daëron et al., 2011; Kluge and Affek, 2012). Initial degassing of CO_2 from water that enters the low pCO_2 cave environment (compared to the high CO_2 levels found in soils) leads to an enrichment in ^{13}C and ^{18}O in DIC and depletion in Δ_{47}. Oxygen isotope exchange between DIC and water drives $\delta^{18}O$ and Δ_{47} back towards equilibrium (Mühlinghaus et al., 2009; Affek, 2013). The progressive precipitation of carbonate minerals further leads to $\delta^{13}C$ and $\delta^{18}O$ values higher than at equilibrium (Scholz et al., 2009; Dreybrodt and Scholz, 2011).

The influence of carbonate precipitation conditions on the isotopic ratios of CCC_{coarse} is not well known. The isotope exchange reaction between water and DIC at the freezing point is much slower ($\tau_{ex} \sim 126{,}000$ s) than chemical reactions and the process of carbonate mineral precipitation ($\tau_p \sim 2000$ s; Dreybrodt and Scholz, 2011). Thus, isotopic values reflecting disequilibrium induced by CO_2 escape from the pool water take a long time to return to isotopic equilibrium ($3 * \tau_{ex} \sim 4.4$ d) and are therefore expected to be recorded in the carbonate minerals.

The aims of this study is to test the applicability of the clumped isotope thermometry (Ghosh et al., 2006; Eiler, 2007, 2011) to CCC_{coarse} precipitated in ice-covered pools. Furthermore, the known CCC_{coarse} formation temperature (~0 °C) can be used together with clumped isotope analyses to assess potential disequilibrium effects in order to improve our understanding of the mode of CCC_{coarse} formation. This is essential in order to extract the potential information of the CCC_{coarse} stable isotopic composition, e.g., for

calculation of the water $\delta^{18}O$ value during carbonate formation.

2. STUDY SITE AND SAMPLES

Cryogenic speleothem samples were selected from several caves in north-western Germany (Herbstlabyrinth-Adventhöhle cave system, Heilenbecker Cave, Hüttenbläserschacht Cave, Malachitdom Cave, Riesenberg Cave) based on petrography, geochemical analyses, and U–Th ages (Table 1). Most caves developed in Devonian Limestone (Riesenberg Cave in Jurassic Limestone) and are located within 200–250 km from each other (Fig. 1A). Today all cave levels are located in the vadose zone with temporally active fluvial systems in the lowest part of the caves. The thickness of the host-rock above the caves, mainly limestone composed of low-Mg calcite, typically reaches 30–50 m (Table 1).

Speleothems actively form today in these caves either as stalagmites, stalactites and flowstones or as floating rafts in small cave pools. The present-day average air temperature in the cave chambers from which the samples were obtained is 9–11 °C.

During the last glacial period the Scandinavian ice sheet terminated 150–400 km from the caves (Fig. 1A), so that they were at least temporarily influenced by permafrost (e.g., Vaikmäe et al., 2001; Renssen and Vandenberghe, 2003; Vandenberghe et al., 2012) with no evidence of glaciation in the cave region itself. Ice accumulation on the cave floor inhibited stalagmite growth and enabled the precipitation of CCC. Due to several large-scale climatic changes (interstadials–stadials) meteoric water could reach the caves and enabled the crystallization of CCC in pools during the freezing process (Žák et al., 2012). Fragments of broken speleothems cemented above the current cave floor are indicative of ice accumulation during glacial times (e.g., Pielsticker, 2000; Kempe, 2004; Richter et al., 2008).

The CCC_{coarse} samples generally consist of several individual grains (Fig. 2, Table 1). Exceptions are braided calcite aggregates from Hüttenbläserschacht Cave and Riesenberg Cave which were large enough to allow multiple clumped isotope analyses on the same sample. The near-stoichiometric calcite CCC_{coarse} show carbon and oxygen isotope compositions similar to slowly precipitating CCC observed in many other central European caves ($\delta^{13}C = -7.0‰$ to $+1.8‰$, $\delta^{18}O$: $-18.1‰$ to $-8.0‰$; Fig. 1B; Richter et al., 2011, 2013).

CCC_{coarse} samples in the Herbstlabyrinth-Adventhöhle cave system were collected from the cave floor and from fissures which dissect a large stalagmite in the Weihnachtsbaum hall. The youngest U–Th age obtained from the stalagmite is 75.8 ± 1.2 ka, whereas the cryogenic calcites on the stalagmite's surface were dated to 23.6 ± 0.3 and 24.0 ± 0.2 ka (Richter et al., 2011). The CCC_{coarse} samples consisted of brown to white rhombohedral calcite crystals with diameters of 1–2 mm, rhombohedral crystal chains with crystal diameters ranging between 0.2 and 3.5 mm (Fig. 2; Richter et al., 2010), and spherolites with a diameter of ~2 mm.

CCC_{coarse} samples from the Malachitdom Cave were collected in the Halligen chamber. The whitish samples have diameters of about 3–4 mm and were dated to 14.5 ± 0.1 and 15.6 ± 0.2 ka (Richter and Riechelmann, 2008). The outer part of the cupula-shaped spherolites was removed prior to analysis of the remaining core.

The CCC_{coarse} sample from the Heilenbecker Cave was collected in the Runden Halle chamber (Richter et al., 2008). The whitish sample has a diameter of 3–4 mm and was dated to 31.3 ± 0.5 ka.

The CCC_{coarse} sample from the Riesenberg Cave was collected in the Neudahmgang chamber. The braided calcite aggregate was part of a larger piece that formed by coalescence of individual CCC grains and has a dimension of ~9 × 15 × 2 mm. Cryogenic carbonates precipitated in Riesenberg Cave between 54 and 66 ka (Richter et al., 2013).

The CCC_{coarse} sample from the Hüttenbläserschacht Cave was collected in the Makkaronihalle chamber. The

Table 1
Details of the investigated caves and CCC_{coarse} samples.

Cave	Hostrock limestone	Elevation of entrance (m a.s.l.)	CCC location below surface (m)	CCC_{coarse} age (ka)	CCC_{coarse} dimensions (mm × mm × mm)	CCC_{coarse} morphology	References
Herbstlabyrinth-Adventhöhle cave system (HA)	Upper Devonian	420	40	23.6–24.0	HA-1: 1–2 × 1–2 × 1	Rhombohedra	Richter et al. (2011)
					HA-2: 4–6 × 2–4 × 1	Rhombohedra chain	
					HA-3: 2 × 2 × 2	Spherolite	
Heilenbecker cave (H)	Middle Devonian	204	50	30.8–31.8	H: 4 × 4 × 3	Spherolite	Richter et al. (2009)
Hüttenbläserschacht cave (HS)	Middle Devonian	185	34	28.6–33.0	HS: 6 × 4 × 3	Braided calcite aggregate	–
Malachitdom cave (M)	Middle Devonian	424	45–50	14.5–15.6	M: 3–4 × 3 × 3	Cupula spherolite	Richter and Riechelmann (2008)
Riesenberg cave (R)	Upper Jurassic	270	35–37	53.7–66.4	R: 15 × 10 × 5	Braided calcite aggregate	Richter et al. (2013)

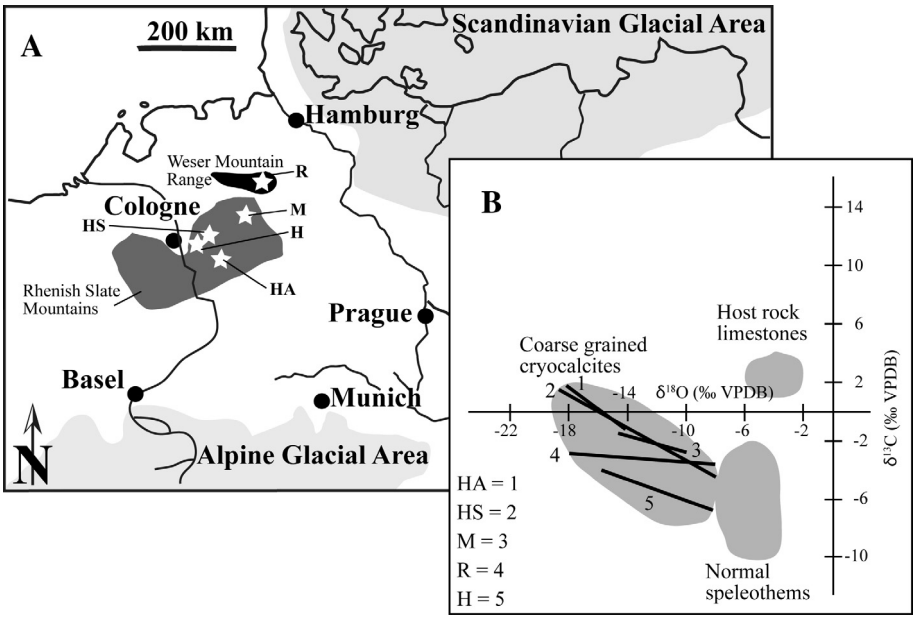

Fig. 1. (A) Locations of the investigated caves with CCC_{coarse} occurrence. During the last glacial period they were situated in the peri-glacial area between the Weichselian ice shield of the Alps to the south and the Scandinavian ice shield in the north. (B) Isotopic signatures of Upper Jurassic (R) and Devonian host rock limestone (H, HA, HS, M), normal speleothems (drip-stones, flow stones) and trend lines of collections of CCC_{coarse} (Richter et al., 2011, 2013). H – Heilenbecker Cave, HA – Herbstlabyrinth-Adventhöhle cave system, HS –Hüttenbläserschacht Cave, M – Malachitdom Cave, R – Riesenberg Cave.

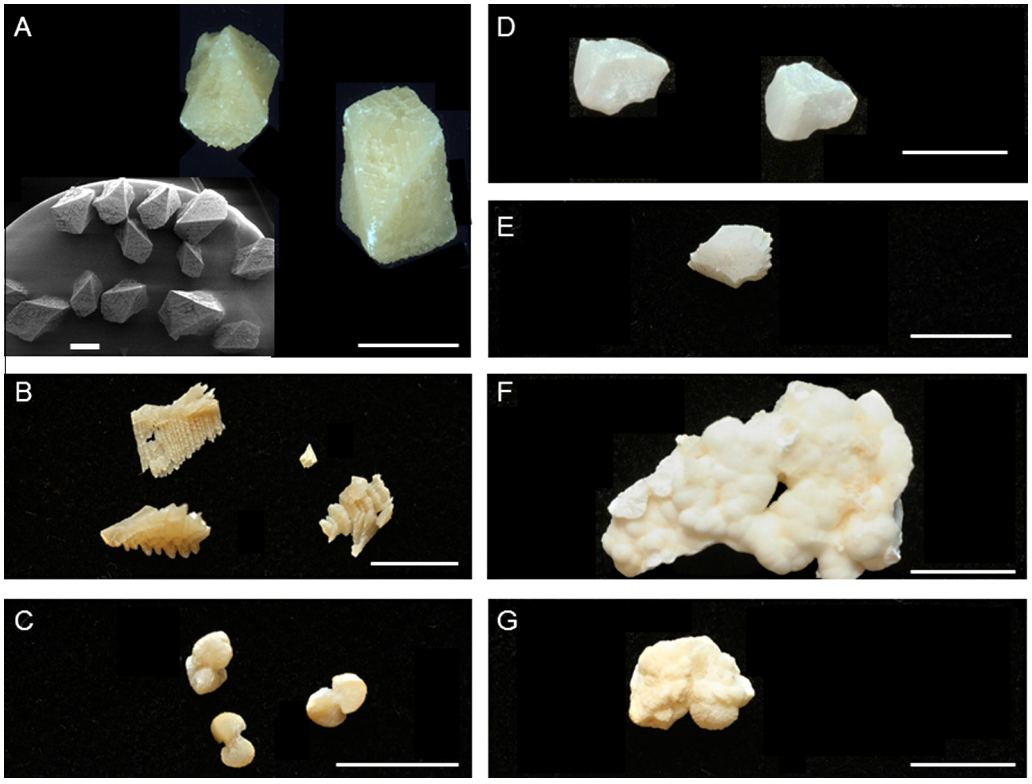

Fig. 2. Photographic images of CCC_{coarse} from different caves in western Germany. (A) Rhombohedral crystals HA-1 from Herbstlabyrinth-Adventhöhle cave system including a scanning electron microscopy image of samples related to HA-1 (with sample holder), (B) rhombohedra chain HA-2 and (C) spherolite HA-3, both from the Herbstlabyrinth-Adventhöhle cave system. (D) Inner cores of cupula spherolites M from Malachitdom Cave, (E) spherolite H from Heilenbecker Cave (F) braided calcite aggregate R from Riesenberg Cave, (G) braided calcite aggregate HS from Hüttenbläserschacht Cave. Both scale bars in A are 1 mm, and 5 mm in B–G.

braided calcite aggregate has a diameter of 3–5 mm and was dated to 29–33 ka.

3. METHODS

3.1. Clumped isotope thermometry

Carbonate clumped isotopes (reported as Δ_{47}) is a measure of chemical bonding between ^{13}C and ^{18}O in the carbonate crystal lattice. At equilibrium it reflects the temperature of the carbonate mineral formation, providing a new paleotemperature proxy (Ghosh et al., 2006; Eiler, 2007, 2011). The main advantage of clumped isotopes for temperature determination compared to the commonly used $\delta^{18}O$ is that it requires no knowledge of the isotopic composition of the solution from which the carbonate mineral precipitates, as Δ_{47} is independent of the $\delta^{13}C$ and $\delta^{18}O$ composition of the carbonate (Cao and Liu, 2012) and therefore of the $\delta^{13}C$ and $\delta^{18}O$ values of the solution.

The isotopologues of nominal mass 47 (mainly ^{13}C–^{18}O–^{16}O) are measured to determine the Δ_{47} parameter by comparing the abundance ratio of mass 47 to mass 44 to that expected at random distribution of the isotopes among all isotopologues (obtained by heating CO_2 to 1000 °C). Δ_{47} is calculated from the measured ratios (R^i) of masses 45, 46 and 47 to mass 44 as:

$$\Delta_{47} = \left[\frac{R^{47}}{2R^{13}\cdot R^{18} + 2R^{17}\cdot R^{18} + R^{13}\cdot \left(R^{17}\right)^2} - \frac{R^{46}}{2R^{18} + 2R^{13}\cdot R^{17} + \left(R^{17}\right)^2} - \frac{R^{45}}{R^{13} + 2R^{17}} + 1 \right] \cdot 1000 \quad (1)$$

The denominator terms are derived by calculating R^{13} ($^{13}C/^{12}C$) and R^{18} ($^{18}O/^{16}O$) from R^{45} and R^{46} assuming random distribution. R^{17} is calculated from R^{18} assuming a mass-dependent relationship between ^{18}O and ^{17}O. Details are given in Affek and Eiler (2006) and Huntington et al. (2009).

Δ_{47} in gas-phase CO_2 is enriched in ^{13}C–^{18}O bonds by ~0.9‰ at 25 °C compared to random distribution, due to the energetically favourable binding of two heavy isotopes at thermodynamic equilibrium (Wang et al., 2004). Carbonates that were formed at Earth surface conditions are less enriched, with typical values of 0.6–0.7‰. A low-temperature Δ_{47}–T relationship (1–50 °C) was first determined empirically by Ghosh et al. (2006) and later refined by Zaarur et al. (2013). We use the Δ_{47}–T relationship of Zaarur et al. (2013) as a reference calibration for the temperature dependence of carbonate precipitated at isotopic equilibrium $\Delta_{47,equil}$ (given in the absolute reference frame of Dennis et al., 2011):

$$\Delta_{47,equil}(T) = 55500/T^2 + 0.0775 \quad (\Delta_{47} \text{ in ‰}, T \text{ in K}) \quad (2)$$

The calibration of Zaarur et al. (2013) is based on a data set that adds several low temperature data points, strengthening the empirical calibration at the temperature interval relevant to this study.

3.2. Analytical procedures

Sample preparation, cleaning and mass spectrometric measurement followed the procedures described by Ghosh et al. (2006), Huntington et al. (2009), and Zaarur et al. (2011). 3–5 mg of speleothem calcite was processed for each measurement. After reaction with phosphoric acid (overnight at 25 °C), evolved CO_2 gas was purified cryogenically and then by passing it in a helium flow through a GC column (Supelco Q-plot) at −20 °C. The analyses were done using a dual-inlet gas-source isotope ratio mass spectrometer (Thermo MAT 253) adapted to analyse masses 44–49 simultaneously.

CCC_{coarse} were measured either as single grains or as a composite of several crystals from the same location. Replicate analyses of individual CCC_{coarse} crystals were generally not feasible due to their small grain size, except for braided calcite aggregates from Riesenberg Cave and Hüttenbläserschacht Cave. CCC_{coarse} samples (Table 1) were measured at different dates between August 2011 and July 2013 to avoid systematic errors from uncharacterized effects associated with short-term fluctuations in mass spectrometric and sample preparation parameters. CO_2 gas (having a range of $\delta^{13}C$ and $\delta^{18}O$ values) that was heated to 1000 °C to achieve random distribution, was measured several times per week following the procedures described by Huntington et al. (2009) to correct for nonlinearity and Δ_{47} scale compression effects. Several standards (Carrara marble, NBS-19, CO_2 gas equilibrated with H_2O at 25 °C, tank-gas 'Corn' CO_2) were prepared and treated the same way as the samples and measured regularly (for details on standardizations see Zaarur et al., 2013). The Δ_{47} values for these standards were defined through an inter-laboratory comparison, with a mean value of the Carrara marble of 0.358 ± 0.003‰ ($n = 64$; Kluge and Affek, 2012).

Δ_{47} values are reported using the newly defined absolute reference frame (Dennis et al., 2011) that is determined by CO_2–H_2O equilibration at different temperatures whose absolute values are defined by gas-phase theory (Wang et al., 2004). The uncertainty of a single clumped isotope measurement is estimated as ±0.02‰ (1σ) based on analysis of standard materials (Carrara marble, NBS-19, Corn cylinder CO_2). Speleothems typically yield a slightly better reproducibility of ±0.010–0.015‰ (Kluge et al., 2013).

Carbon and oxygen isotope values were defined using a pre-calibrated Oztech reference gas ($\delta^{13}C = -3.64$‰ VPDB, $\delta^{18}O = -15.80$‰ VPDB; Safford, AZ, USA) and verified by regular measurements of NBS-19. The mean $\delta^{18}O$ of NBS-19 measurements from January 2010 to February 2012 is -2.17 ± 0.04‰ (VPDB, $n = 13$, 1σ standard deviation), in agreement with the NIST reference value of −2.2‰. Carbon isotopes are slightly more enriched (2.09 ± 0.11‰, VPDB, $n = 13$, 1σ standard deviation) than the NIST reference of 1.95‰ (VPDB). The typical standard deviation in $\delta^{13}C$ and $\delta^{18}O$ for replicate sample analysis is 0.1–0.2‰ with standard errors of about 0.06‰. All carbonate data is reported with respect to VPDB and water with respect to VSMOW.

The conversion of $CaCO_3$ $\delta^{18}O$ to water $\delta^{18}O$ is based on the temperature T (here assumed to be ~0 °C) and the canonical equilibrium fractionation factor given by Kim and O'Neil (1997) corrected for the acid reaction fractionation (Böhm et al., 2000; Affek et al., 2008):

$$1000 \ln \alpha_{calcite-H_2O} = 18.03 \times 10^3 / T - 32.17 \quad (3)$$

U-series dating of cryogenic crystals was performed at the Max-Planck-Institute for Chemistry, Mainz (Germany) using a MC-ICPMS following the technique of Hoffmann et al. (2007) and at the Heidelberg Academy of Sciences (Germany) using a thermal ionization mass spectrometer (TIMS) following the technique of Scholz and Hoffmann (2008). Samples from Herbstlabyrinth, Heilenbecker, and Malachitdom Cave were dated at the Heidelberg Academy of Sciences; CCCs from Riesenberg and Hüttenbläserschacht Cave at the Max-Planck-Institute for Chemistry, Mainz.

4. RESULTS

Average Δ_{47} values of the CCC_{coarse} replicate means of samples from different caves vary between $0.734 \pm 0.017‰$ ($n = 2$) and $0.803 \pm 0.010‰$ ($n = 5$; Table 2). Using Eq. (2) this corresponds to an apparent temperature range of 3 ± 3 to 18 ± 4 °C. The temperature uncertainty includes the uncertainty in the Δ_{47}-temperature calibration relationship (~2 °C; Zaarur et al., 2013). In comparison, the expected Δ_{47} value at the water freezing point (0 °C) is $0.821 \pm 0.015‰$.

Measured calcite $\delta^{18}O$ values are extremely negative and vary between −17.94‰ and −11.32‰; $\delta^{13}C$ shows a lower variability with values between −3.38‰ and +0.79‰. Combining calcite $\delta^{18}O$ values with the expected freezing temperature of pool water (0 to −1 °C) and assuming equilibrium carbonate precipitation results in calculated water $\delta^{18}O_w$ values between −21.3‰ and −14.7‰ using Eq. (3). Uncertainties are ±0.1–0.2‰ based on the range of expected freezing temperatures (0 to −1 °C). For reference, modern-day rainfall in the investigated region has an annual mean $\delta^{18}O_w$ value of −7‰ to −8‰ VSMOW (IAEA/WMO, 2013).

5. INTERPRETATION AND DISCUSSION

We use clumped isotopes to study the formation mechanism of CCC_{coarse} and examine the assumption of their formation under isotopic equilibrium, in comparison with disequilibrium processes recognized in stalagmites. We briefly review the relevant formation mechanism and processes that determine the isotopic values of 'normal' speleothems such as stalagmites, and compare them to pool precipitates. The pool environment is of specific interest as CCC_{coarse} particles are formed in small pools under slow freezing conditions (e.g., Žák et al., 2008).

5.1. Stalagmite formation mechanisms

Stalagmites grow by carbonate deposition from a thin water film (~100 μm) that is fed by super-saturated water dripping on the stalagmite top (Dreybrodt, 1980). CO_2 degassing from the water film induces super-saturation with respect to $CaCO_3$ and enables carbonate precipitation. The oxygen isotope ratio that is then recorded in the stalagmite depends on multiple parameters such as the drip water $\delta^{18}O$ value, drip rate, CO_2 gradient between drip water and cave, and temperature (e.g., Lachniet, 2009; Mühlinghaus et al., 2009; Scholz et al., 2009; Dreybrodt and Scholz, 2011). Many speleothems exhibit a non-equilibrium oxygen isotope signature (Mickler et al., 2006; McDermott et al., 2011; Tremaine et al., 2011). Focusing on the processes at the stalagmite top, the disequilibrium can be related to the initial CO_2 degassing, that proceeds within <10 s and leaves the DIC significantly ^{18}O enriched until it is re-equilibrated by exchange with the water isotopes through hydration/dehydration of CO_2 at timescales of 6200 (25 °C) to 126,000 s (0 °C; Dreybrodt and Scholz, 2011). An additional source of ^{18}O enrichment is the Rayleigh-type evolution of the DIC during carbonate precipitation (Scholz et al., 2009). Carbonate precipitation in a thin water film can be rapid (2000 s at 0 °C; Dreybrodt and Scholz, 2011), not allowing sufficient time for full isotope exchange between the DIC species and water.

5.2. Speleothem formation in cave pools

Several types of speleothems form in cave pools such as rafts that precipitate directly at the pool surface and larger crystals that form below the water surface at the pool rim. Raft crystals are formed at the interface between water and the cave atmosphere in a thin boundary layer. Their formation therefore follows similar constraints as in stalagmites. In contrast, subaqueous mineral

Table 2
Average carbonate Δ_{47}, $\delta^{13}C$ and $\delta^{18}O$ values of studied CCC_{coarse} samples. $\Delta_{47,abs}$ is the clumped isotope value in the absolute reference frame (Dennis et al., 2011), T is the apparent temperature calculated from clumped isotopes using Eq. (2). Uncertainties are given as standard error. The temperature uncertainty includes the uncertainty of the Δ_{47}–T thermometer calibration (~2 °C, Zaarur et al., 2013).

Sample	Replicates	$\Delta_{47,abs}$ (‰)	$\delta^{13}C$ (‰)	$\delta^{18}O$ (‰)	T (°C)
HA-1	5	0.803 ± 0.010	−1.81 ± 0.15	−15.72 ± 0.13	3 ± 3
HA-2	5	0.756 ± 0.010	−1.78 ± 0.04	−16.33 ± 0.08	13 ± 3
HA-3	2	0.763 ± 0.026	−0.70 ± 0.06	−17.94 ± 0.13	11 ± 5
H	2	0.734 ± 0.017	−3.38 ± 0.08	−15.49 ± 0.11	18 ± 4
HS	5	0.758 ± 0.007	−2.78 ± 0.03	−14.20 ± 0.06	12 ± 2
M	6	0.743 ± 0.006	−2.04 ± 0.02	−13.46 ± 0.04	16 ± 2
R	4	0.743 ± 0.004	0.79 ± 0.08	−11.32 ± 0.21	16 ± 2

growth in such pools (e.g., of pool crystals) is substantially different in that the CO_2 degassing is orders of magnitude slower. At 10 °C and a water depth of 1 cm the time required for CO_2 to diffuse through the water column and degas is $\sim 3.6 \times 10^4$ s instead of 3.5 s at the 100 μm thick water film on a stalagmite (calculation based on a molecular diffusion coefficient of 1.13×10^{-5} cm^2/s; Dreybrodt and Scholz, 2011). This affects the reaction rates and the isotopic evolution of the DIC, generally leading to lower growth rates of subaqueously formed precipitates, potentially allowing for buffering of the $\delta^{18}O$ and Δ_{47} through isotope exchange with water. Experiments simulating speleothem growth in pools found $\delta^{18}O$ values in equilibrium with the solution, as a result of effective DIC-water isotope exchange (Wiedner et al., 2008). In contrast, $\delta^{13}C$ values were significantly enriched, inversely proportional to the water depth, as a result of the degassing carbon isotope signal not being buffered (Wiedner et al., 2008).

5.3. Speleothem formation under freezing conditions in cave pools

Carbonate minerals that form in freezing pools have been investigated using their $\delta^{18}O$ and $\delta^{13}C$ values. In this study we use these together with clumped isotopes to examine the formation process of CCC_{coarse}. Based on their morphology and the very low $\delta^{18}O$ values observed in CCC_{coarse} they were suggested to precipitate slowly in pools under freezing conditions (Žák et al., 2008, 2012). In the following we highlight some of the physical and chemical conditions related to this specific environment that make CCC_{coarse} different from 'normal' speleothems.

Water entering a cave whose temperature is constantly below the freezing point is quickly disconnected from the cave air as the water freezes at the pool surface, creating an ice cover. The rate of further freezing depends on several parameters such as the temperature of the cave chamber and the volume of water in the pool. Thin water films in shallow pools freeze rapidly and lead to the precipitation of CCC_{fine}. The gradual freezing of larger water bodies (on the order of 10–1000 liters with water depths exceeding a few cm) proceeds similarly fast at the beginning, but later slows down significantly. The heat released during the phase transition of water to ice (3.3×10^5 J/kg; Haynes et al., 2012) is less efficiently dissipated as ice thickness increases, leading to the slowing of the freezing process. The temperature of the water, which at isotopic equilibrium is recorded in the composition of the CCC_{coarse}, is thus expected to be ~0 °C.

Slow freezing leads to a gradual increase in super-saturation due to ions being rejected from the ice and enables mineral growth that result in carbonate crystals reaching dimensions of several mm to few cm (Žák et al., 2008). The observed sizes of CCC_{coarse} minerals provide a first-order constraint on the minimum volume of the pool water. For example, assuming initial HCO_3^- and Ca^{2+} concentrations of 140 and 70 mg/l, respectively, which are typical values in modern drip water in caves in the study area (Riechelmann et al., 2011), about 1 liter of water is necessary for the formation of one $3 \times 3 \times 3$ mm^3 crystal. Drip water during glacial periods likely had lower ionic concentrations due to reduced microbial activity in the soil (e.g., Pieitkäinen et al., 2005), or even lacking soil, and therefore required larger pool volumes to precipitate comparable crystals. Size and isotopic differences amongst the studied CCC_{coarse} samples were likely related to differences in pool volume, freezing rates and the evolution of super-saturation.

As water freezes ^{18}O preferentially accumulates in the ice, so that the remaining water becomes gradually ^{18}O depleted (O'Neil, 1968; Lehmann and Siegenthaler, 1991). At equilibrium, $\delta^{18}O$ values of the CCC_{coarse} are expected to follow the time evolution of the water and it, therefore, also varies with pool size and the extent of freezing. The variability that we observe in $\delta^{18}O$, thus, cannot be taken as evidence for disequilibrium. Clumped isotopes, in contrast, reflect water temperature, irrespective of the amount of water and its composition. Δ_{47} values below that expected at equilibrium at 0 °C (Section 5.4) together with the variability in Δ_{47} values suggests a variable degree of disequilibrium (see discussion below).

During freezing, large molecules, ions and gases (e.g., $Ca^{2+}, HCO_3^-, CO_2, Ar$) are rejected from the ice as they do not fit into its lattice and accumulate in the remaining water. The concentrations of Ca^{2+} and HCO_3^- increase until nucleation and precipitation of carbonate crystals starts. The temporal evolution of the Ca^{2+} and HCO_3^- concentrations is primarily determined by the rate of water freezing versus the rate of carbonate precipitation. In contrast to 'normal' speleothem formation, the initial solution does not need to be super-saturated and exhibits a significantly different temporal evolution of the HCO_3^- and Ca^{2+} concentrations. Whereas for stalagmites these concentrations strongly decrease within the time interval between consecutive drips due to mineral formation, in a freezing pool they can be constant or even increase during precipitation of CCC_{coarse} due to the steady expulsion of ions from the gradually forming ice. The temporal evolution of the super-saturation affects the evolution of the $CaCO_3$ precipitation rate and potentially the isotopic composition of CCC_{coarse}.

Gas exchange between water and cave air in the case of CCC_{coarse} formation is very different from that during stalagmite growth. When a cave pool is covered by ice, gas exchange is attenuated and CO_2 cannot escape easily to the cave atmosphere. In such conditions it is expected that CO_2 degassing will be slow, potentially allowing sufficient time for oxygen and clumped isotope buffering prior to $CaCO_3$ precipitation. The formation of each $CaCO_3$ molecule is associated with the generation of a CO_2 molecule that accumulates in the solution (Killawee et al., 1998). Without gas exchange carbonate precipitation slows down and would finally cease. During ice formation gas molecules are rejected from the ice (Namiot and Bukhgalter, 1965; Craig et al., 1992) and accumulate in the water, which can lead to bubble nucleation. CO_2 created during carbonate precipitation may diffuse into these bubbles or escape through cracks in the ice. This pathway for CO_2 degassing is likely relevant only in late stages of freezing.

5.4. Clumped isotope data

Clumped isotopes have been shown to be a sensitive indicator for disequilibrium in stalagmites. Kinetic isotope effects during rapid CO_2 degassing lead to higher $\delta^{18}O$ and $\delta^{13}C$ values, but lower Δ_{47} values (Guo, 2008). In modern speleothems correlations between higher $\delta^{18}O$ and lower Δ_{47} values were observed (Daëron et al., 2011; Wainer et al., 2011; Kluge and Affek, 2012; Kluge et al., 2013). A stronger disequilibrium is manifested by decreased Δ_{47} values, corresponding to higher apparent temperatures. As clumped and oxygen isotopes are closely linked, disequilibrium in the Δ_{47} value is also indicative of oxygen isotope disequilibrium (Affek, 2013). We use the same approach here to test for equilibrium in CCC_{coarse}. In spite of suggestions that the attenuated degassing and slow calcite precipitation in ice covered pools enable isotopic equilibrium (Žák et al., 2004, 2012), our data suggests disequilibrium also in CCC_{coarse}. Except for one sample for which the Δ_{47} value is within error of the expected 0 °C equilibrium value, our data shows varying degrees of disequilibrium with clumped isotope-derived temperatures between 3 ± 3 and 18 ± 4 °C (Fig. 3). Possible causes for disequilibrium can be examined by the relationship between Δ_{47} and $\delta^{18}O$ and $\delta^{13}C$ values.

Δ_{47} offsets calculated relative to the expected equilibrium Δ_{47} value at 0 °C of 0.821‰ show no correlation with $\delta^{13}C$ values (Fig. 4A). The positive $\delta^{13}C$ values are consistent with Rayleigh fractionation within the DIC (see Section 5.5), but provide no further information about the causes of the observed disequilibrium. In contrast, Δ_{47} offsets show a weak correlation with $\delta^{18}O$ values ($R^2 = 0.37$, Fig. 4B). The correlation is weaker than that observed in stalagmites probably due to non-degassing related variability in $\delta^{18}O$. Whereas some of the scatter might be due to differences in the initial water $\delta^{18}O$ values at the different caves before freezing (for example, the meteoric precipitation $\delta^{18}O$ values vary today by about 1‰ in the study region; IAEA/WMO, 2013), significant $\delta^{18}O$ variations are expected due to differences in pool size and in the water fraction being frozen in each pool.

The Δ_{47}-$\delta^{18}O$ correlation of our CCC_{coarse} data shows that a decrease of 0.005 (±0.003)‰ in Δ_{47} corresponds to an increase of 1‰ in $\delta^{18}O$ values (Fig. 4B). This value is lower than determined for CO_2 hydration or hydroxylation combined with carbonate formation (0.020–0.026; Guo, 2008) and significantly lower than trends observed in 'normal' speleothems (0.04–0.06; Daëron et al., 2011; Wainer et al., 2011; Kluge et al., 2013). The Δ_{47}-$\delta^{18}O$ slope in CCC_{coarse} is strongly affected by the ^{18}O depletion due to water freezing that counteracts the degassing-related ^{18}O enrichment.

Rapid CO_2 degassing, which is the main process causing disequilibrium in the thin films of stalagmites, is also a potential source of disequilibrium in CCC_{coarse} and could occur via rapid gas loss through bubble formation or through cracks in the ice cover. Alternatively, fast mineral growth may lead to disequilibrium due to kinetic fractionation between remaining HCO_3^- and CO_2 that evolved during $CaCO_3$ formation, whereas slow growth minimizes disequilibrium by allowing buffering. Samples R and M are the largest samples and exhibit a microcrystalline structure that suggest fast growth. These samples show the largest Δ_{47} offsets. In contrast, sample HA1 consists of rather large rhombohedral crystals, indicative of relatively slow growth, and

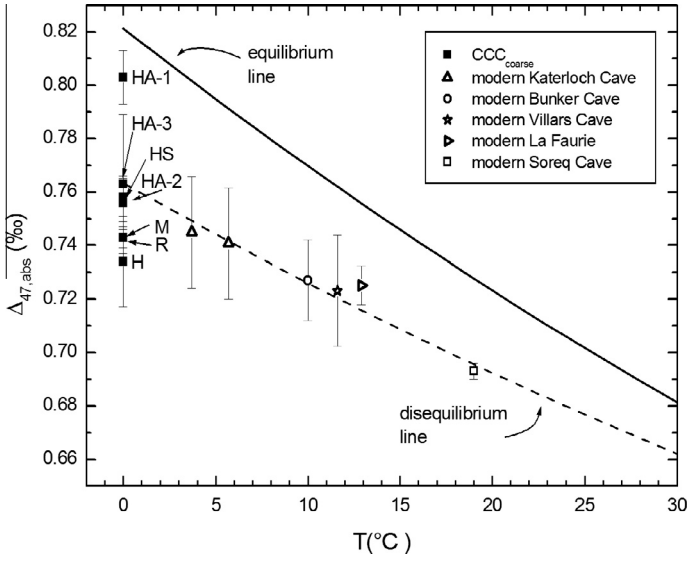

Fig. 3. Δ_{47} values of CCC_{coarse} (this study, filled squares) compared to the Δ_{47}–T relationship of equilibrium precipitation (Zaarur et al., 2013, black line) and data from vadose speleothems. CO_2 degassing from thin water films leads to offsets from equilibrium towards lower Δ_{47} (higher temperatures) which is visible in modern stalagmites (open symbols) from Villars, La Faurie and Katerloch Cave (Daëron et al., 2011), the Bunker Cave region (Kluge et al., 2013), and Soreq Cave (Affek et al., 2008). The dashed line is a linear fit (of Δ_{47} versus $1/T^2$) to modern speleothem deposits ($4.02 \times 10^4/T^2 + 0.225$; T in K).

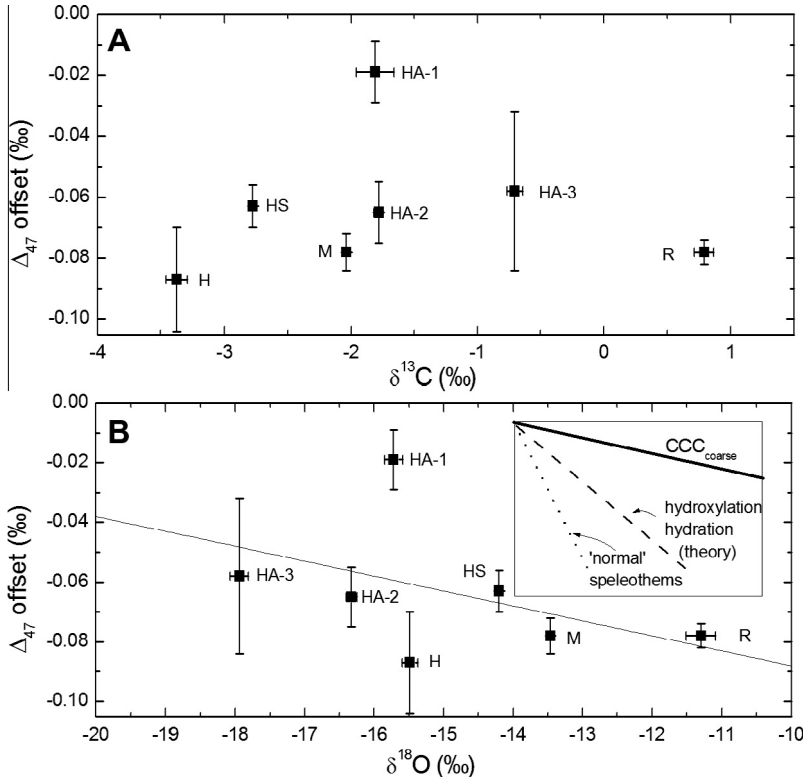

Fig. 4. Δ_{47} offsets versus $\delta^{13}C$ (A) and $\delta^{18}O$ (B) values of CCC_{coarse}. Whereas no trend is visible for $\delta^{13}C$, more negative $\delta^{18}O$ values are linked to a reduced Δ_{47} offset. The inset in B shows the Δ_{47}-$\delta^{18}O$ slope of the CCC_{coarse} (thick black line) together with the theoretical slope for hydration and hydroxylation at 0 °C (dashed black line; Guo, 2008) and observations from 'normal' vadose speleothems, e.g., stalagmites (dotted black line; Kluge et al., 2013).

is closest to the expected Δ_{47} equilibrium values. Sample M provides a window into early CCC_{coarse} formation as the outer layer, corresponding to late crystal growth, was removed prior to analysis. Sample M shows one of the highest Δ_{47} offset and suggests that the isotopic disequilibrium is higher at the start of CCC_{coarse} precipitation. It is possible that the isotopic disequilibrium is due to initial CO_2 degassing before the cave pool is sealed by an ice cover. Oxygen isotope exchange between DIC and water is not fast enough to reach isotopic equilibrium before mineral formation starts. Δ_{47} values that are even lower than those observed in stalagmites (Fig. 3) are likely due to the increasing difference between the time scales of degassing and isotopic equilibration between DIC and water at lower temperatures (see e.g., Dreybrodt and Scholz, 2011). This makes the degassing-related disequilibrium dominant at freezing temperatures and causes large offsets from expected equilibrium Δ_{47} values in early-formed CCC.

5.5. Oxygen and carbon isotope ratios of CCC_{coarse}

CCC_{coarse} $\delta^{18}O$ (-17.94 ± 0.13‰ to -11.32 ± 0.21‰) and $\delta^{13}C$ values (-3.38 ± 0.08‰ to $+0.79 \pm 0.08$‰) of this study are similar to previously published CCC_{coarse} measurements at these caves ($\delta^{18}O$: -18.1‰ to -8.0‰, $\delta^{13}C$: -7.0‰ to $+1.8$‰; Richter et al., 2011, 2013) and are consistent with CCC_{coarse} values from other central European caves ($\delta^{18}O$: -24‰ to -10‰, $\delta^{13}C$: -9‰ to $+6$‰; e.g., Žák et al., 2012). The CCC_{coarse} samples of our study follow a generally negative trend between $\delta^{18}O$ and $\delta^{13}C$ values (Fig. 5). The $\delta^{18}O$–$\delta^{13}C$ slope has a value that agrees with observations of CCC_{coarse} from other European caves (Žák et al., 2012).

This $\delta^{18}O$–$\delta^{13}C$ correlation can be explained by considering Rayleigh fractionation of the DIC due to $CaCO_3$ precipitation together with the gradual depletion of the water oxygen isotopes (Figs. 6 and 7). The evolution of isotopic values under Rayleigh fractionation was calculated using the following equation (e.g., Mook, 2000):

$$\delta^x = (1 + \delta^x_{ini}) \cdot f^{\alpha-1} - 1 \quad (4)$$

δ^x is the isotopic value (in ‰) that is related to the remaining liquid fraction f ($0 < f < 1$) for water or to the HCO_3^- fraction in the DIC. The original fluid (or HCO_3^- in the pool water) has the isotopic value δ^x_{ini}. The fractionation factors used are given in Table 3.

Gradual freezing of pool water preferentially traps ^{18}O in the ice and results in a gradual decrease in ^{18}O within the small amount of water remaining (Fig. 6). Carbonates precipitated from pool water follow the trend in water composition when precipitation is slow enough to allow full oxygen isotope exchange between DIC and water (Fig. 6). Slow CCC precipitation in a late stage of pool freezing therefore results in the most negative $\delta^{18}O$ values. At the early stages precipitation is likely faster so that isotope exchange with water may be limited and DIC may be affected

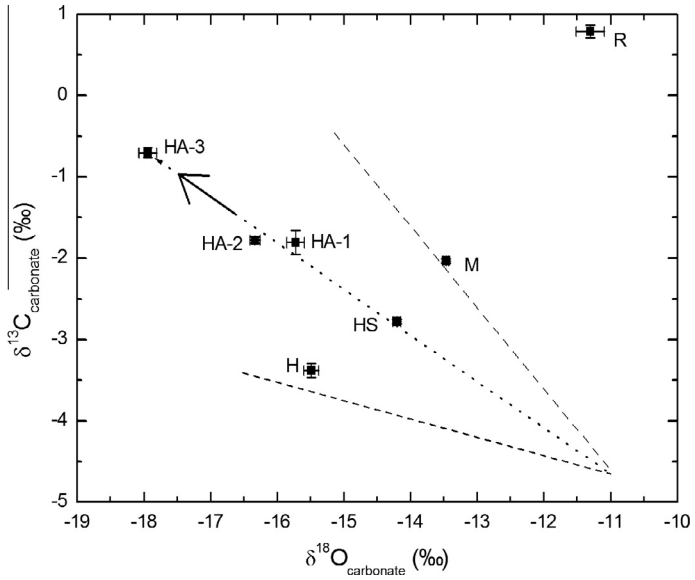

Fig. 5. $\delta^{18}O$ and $\delta^{13}C$ values of CCC_{coarse} from the investigated caves. The dotted line is given for reference and indicates an intermediate $\delta^{13}C$–$\delta^{18}O$ trend relative to that of CCC_{coarse} in central Europe (Žák et al., 2012). The dashed lines illustrate the minimum and maximum values of the $\delta^{13}C$ and $\delta^{18}O$ trends of CCC_{coarse} in Žák et al. (2012). The arrow points towards progressive freezing of pool water combined with carbonate precipitation.

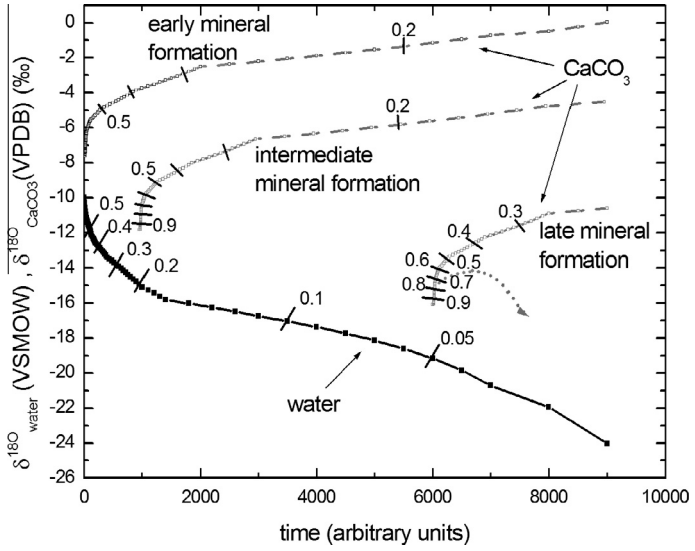

Fig. 6. Water $\delta^{18}O$ (thick black line) and carbonate $\delta^{18}O$ values (grey dashed lines). The fractions of remaining HCO_3^- and water are indicated by the numbers on the graph. Carbonate $\delta^{18}O$ values are calculated via Rayleigh fractionation (Eq. (4)) and the assumption of negligible isotopic exchange with water after the precipitation started (see Sections 5.3 and 5.5 for details and Table 3 for the fractionation factors used). Carbonate precipitation and water freezing was assumed to slow down progressively. Late carbonate precipitation leads to more negative $\delta^{18}O$ values due to the more ^{18}O-depleted water (illustrated for three examples of early, intermediate and late mineral formation). Oxygen isotope buffering of DIC and precipitated carbonate is indicated schematically by a dotted grey curve.

by degassing when the pool is not yet completely covered by ice. Fig. 7A and B gives a schematic description of the correlation between $\delta^{13}C$ and $\delta^{18}O$ values in both end-member cases. Disregarding oxygen isotope exchange between DIC and water after precipitation started, $\delta^{13}C$ and $\delta^{18}O$ values of CCC_{coarse} follow a simple Rayleigh fractionation trend towards more positive $\delta^{13}C$ and $\delta^{18}O$ values (Fig. 7, line A). When DIC-water isotope exchange is effective (Fig. 7, line B), i.e. during slow $CaCO_3$ formation, $\delta^{18}O$ values in the carbonate would instead tend to lower values as a result of the strong water ^{18}O-depletion. In this case strongly negative $\delta^{18}O$ values are correlated with a marginal increase in $\delta^{13}C$ values.

The actual $\delta^{18}O$–$\delta^{13}C$ trend is influenced by the growth rate, that depends on the super-saturation that in turn reflects the evolution of the HCO_3^- and Ca^{2+} concentration, and by the isotope exchange with water. Depending on the mineral growth rate, which determines the fraction of

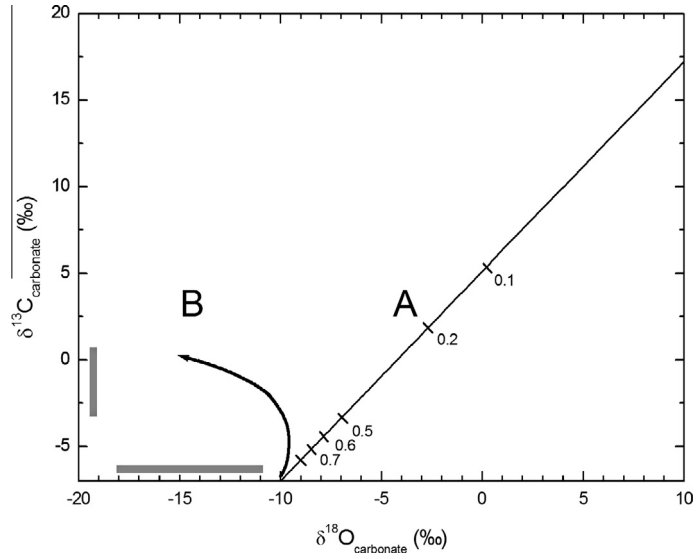

Fig. 7. Isotopic evolution of CCC_{coarse} precipitates. (A) Isotopic evolution of carbonates calculated from the Rayleigh fractionation between HCO_3^- and $CaCO_3$, H_2O and CO_2 (see Sections 5.3 and 5.5 for details and Table 3 for the fractionation factors used). Exchange of oxygen isotopes between water and DIC is disregarded here. The fraction of HCO_3^- remaining is indicated on the graph. (B) as in (A) but combined with $\delta^{18}O$ buffering of the DIC isotopes with water. The grey bars at the axes indicate the range of measured CCC_{coarse} values.

Table 3
Fractionation factors used. Each mole of carbonate is related to the release of one mole of CO_2 during mineral formation. The oxygen atoms of the bicarbonate are partitioned between $CaCO_3$, CO_2 and H_2O. The combined fractionation factor $^{18}\alpha$ is calculated from the different components using their relative contribution to the reaction (1/6 for H_2O, 2/6 for CO_2, 3/6 for $CaCO_3$; Scholz et al., 2009).

Fractionation	Value at 0 °C	References
$^{18}\alpha$ (water/ice)	1.0029	O'Neil (1968), Lehmann and Siegenthaler (1991)
$^{18}\alpha$ (HCO_3^-, H_20)	0.9627	Beck et al. (2005)
$^{18}\alpha$ (HCO_3^-, $CaCO_3$)	0.9974	Mook (2000), Beck et al. (2005)
$^{18}\alpha$ (HCO_3^-, $CO_{2,gas}$)	1.0093	Mook (2000), Beck et al. (2005)
$^{18}\alpha$ (HCO_3^-, $CO_{2,aq}$)	1.0086	Mook (2000), Beck et al. (2005)
Combined $^{18}\alpha$ ($HCO_3^- \rightarrow H_20, CaCO_3, CO_{2,aq}$)	0.9953	
Combined $^{18}\alpha$ ($HCO_3^- \rightarrow H_20, CaCO_3, CO_{2,gas}$)	0.9956	
$^{13}\alpha$ (HCO_3^-, $CaCO_3$)	0.9996	Mook (2000)
$^{13}\alpha$ (HCO_3^-, $CO_{2,gas}$)	0.9892	Mook et al. (1974)
$^{13}\alpha$ (HCO_3^-, $CO_{2,aq}$)	0.9880	Mook (2000)
Combined $^{13}\alpha$ ($HCO_3^- \rightarrow CaCO_3, CO_{2,aq}$)	0.9938	
Combined $^{13}\alpha$ ($HCO_3^- \rightarrow CaCO_3, CO_{2,gas}$)	0.9944	

DIC precipitated at each time step, carbonate $\delta^{18}O$ either follows closely the trend of water $\delta^{18}O$ or is decoupled. At the start of CCC_{coarse} precipitation, water may be strongly super-saturated leading to fast mineral growth that slows down as the reaction proceeds and super-saturation decreases. Whereas the isotopic evolution initially follows a Rayleigh process within the DIC with precipitation rate being too high to allow complete oxygen isotope exchange with water, the DIC $\delta^{18}O$ will gradually equilibrate with water when mineral growth rate decreases (schematically illustrated in the dashed line in Fig. 6 and Fig. 7 B).

The observed trend of CCC_{coarse} $\delta^{18}O$ values becoming more negative combined with increasingly positive $\delta^{13}C$ values suggests the effect of DIC utilization to be small (but not negligible) compared to that of water freezing. Using a carbonate $\delta^{13}C$ value of $-7‰$ for the first crystals to form, a value typical for 'normal' speleothem $\delta^{13}C$ in the study area (Žák et al., 2012), measured $\delta^{13}C$ values suggest (through a Rayleigh fractionation calculation; Eq. (4), Table 3) that 25–56% of the DIC is utilized relative to the initial HCO_3^- concentration. The fraction of DIC utilized cannot be estimated from the carbonate $\delta^{18}O$ value as the initial water $\delta^{18}O$ value at the beginning of the mineral formation is not known and oxygen isotope exchange with water constantly modifies the $\delta^{18}O$ value of the remaining HCO_3^-.

Δ_{47} values reflect here the degree of disequilibrium, in contrast to the carbonate $\delta^{18}O$ values that, in general, are dominated by the oxygen isotope fractionation between water and ice and the resulting enrichment of ^{18}O in the ice. The carbonate $\delta^{18}O$ values also contain a disequilibrium component as observed by clumped isotope measurements, but they are modified by oxygen isotope exchange between DIC and water. Calculating the extent of freezing

from the carbonate $\delta^{18}O$ values is therefore impossible, except when Δ_{47} values suggest mineral precipitation under equilibrium conditions.

Based on its Δ_{47} value sample HA-1 is within analytical uncertainty from equilibrium and, therefore, $\delta^{18}O$ in that sample reflects DIC that is in equilibrium with water. The pool water composition can be estimated using the CCC_{coarse} oxygen isotope data, and then used in a Rayleigh fractionation approach (Eq. (4)) to estimate the fraction of unfrozen pool water. Further, the water entering the cave is assumed to have a $\delta^{18}O$ value of −13‰. This estimate is based on modern drip water in western German caves (e.g., Bunker Cave, about −8‰; Riechelmann et al., 2011) and the $\delta^{18}O$ difference of about 5‰ between the Holocene and 15.5 ka (a cold period at the end of the Late Glacial) recorded by benthic ostracods of a lake in southern Germany (von Grafenstein et al., 1999). Using the oxygen isotope thermometer equation (Eq. (3)) and the Rayleigh distillation relationship (Eq. (4)) we obtain a remaining water fraction of 13% for HA-1. The actual extent of water freezing was likely slightly higher, as the carbonate $\delta^{18}O$ values also included a component related to the decrease in the DIC concentration (due to mineral formation and potential CO_2 degassing) and possibly a small associated disequilibrium component that further increased the carbonate $\delta^{18}O$ value. The observation that the sample closest to isotopic equilibrium is associated with a pool that is almost completely frozen (namely, a small fraction of remaining water) is consistent with suggestions of a robust ice cover that leads to attenuated degassing and therefore slow calcite precipitation.

Our study shows that a quantitative interpretation of CCC_{coarse} carbon and oxygen isotope values is hampered due to potential disequilibrium effects. Δ_{47} measurements can be used to distinguish between equilibrium and disequilibrium precipitation and can assist in determining if a specific sample was formed under freezing conditions, i.e., if the sample Δ_{47}-based temperature is consistent with 0 °C. Δ_{47} temperatures above 0 °C, however, do not refute a cryogenic origin, but generally reflect disequilibrium effects. In case of equilibrium precipitation $\delta^{13}C$ and $\delta^{18}O$ values give information about the details of mineral formation and allow an estimate of the extent of pool freezing. However, even then estimating $\delta^{18}O$ of initial pool water requires knowing the extent of freezing that at this stage cannot be determined independently.

6. CONCLUSION

We use clumped isotope measurements in combination with traditional $\delta^{18}O$ and $\delta^{13}C$ analyses to constrain the formation mechanisms of CCC_{coarse}. Super-saturation of the precipitating solution is achieved and maintained by ion rejection from the forming ice, although in some cases it may include also degassing of CO_2 as in 'normal' (vadose) speleothems. Δ_{47} values in CCC_{coarse} from western Germany yield apparent formation temperatures higher than expected from slowly freezing pool water, mostly indicating isotopic disequilibrium during carbonate formation. The unusually negative $\delta^{18}O$ values of this type of CCC, attributed to the isotopic fractionation between water and ice, follow a trend towards more negative $\delta^{18}O$ values combined with reduced Δ_{47} offset. Namely, CCC_{coarse} that precipitated during a late stage of pool freezing correspond to more negative $\delta^{18}O$ values and reduced Δ_{47} offsets, suggesting a trend towards isotopic equilibrium. The observed isotopic disequilibrium in CCC_{coarse} can be due to initial CO_2 degassing before pool water freezing, CO_2 partitioning into gas bubbles in a later stage, or kinetic fractionation during periods of faster mineral growth. The CCC_{coarse} trend of slightly reduced Δ_{47} offsets when $\delta^{18}O$ values are more negative suggests that the initial disequilibrium significantly influences the calcite composition, similar to the stalagmite formation process where Δ_{47} and $\delta^{18}O$ disequilibrium is mainly caused by rapid initial CO_2 degassing from the thin film of drip water.

ACKNOWLEDGEMENTS

The research was funded by the German Science Foundation DFG (Forschungsstipendium KL2391/1-1 to Tobias Kluge) and the National Science Foundation (NSF-EAR-0842482 to Hagit P. Affek). We thank Shikma Zaarur, Casey Saenger, and Peter Douglas for fruitful discussions, Glendon Hunsinger of the Earth System Center for Stable Isotope Studies of the Yale Institute for Biospheric Studies for technical assistance, Eric Lazo-Wasem of the Yale Peabody Museum for imaging of HA-1, and Nick Longrich for assistance in imaging of HA-2, -3, H, HS, M, and R. We are grateful for thoughtful comments of three anonymous reviewers that helped to improve the manuscript.

REFERENCES

Affek H. P. (2012) Clumped isotope paleothermometry: Principles, applications and challenges. In Earth's deep time climate – the state of the art in 2012. Paleontological Society Papers (eds. L. C. Ivany and B. T. Huber), The Paleontological Society, Vol. 18, pp. 101–114.

Affek H. P. (2013) Clumped isotopic equilibrium and the rate of isotope exchange between CO_2 and water. *Am. J. Sci.* **313**, 309–325.

Affek H. P. and Eiler J. M. (2006) Abundance of mass 47 CO_2 in urban air, car exhaust and human breath. *Geochim. Cosmochim. Acta* **70**, 1–12.

Affek H. P., Bar-Matthews M., Ayalon A., Matthews A. and Eiler J. M. (2008) Glacial/interglacial temperature variations in Soreq cave speleothems as recorded by 'clumped isotope' thermometry. *Geochim. Cosmochim. Acta* **72**, 5351–5360.

Beck W. C., Grossman E. L. and Morse J. W. (2005) Experimental studies of oxygen isotope fractionation in the carbonic acid system at 15, 25 and 40 °C. *Geochim. Cosmochim. Acta* **69**, 3493–3503.

Böhm F., Joachimski M. M., Dullo W. C., Eisenhauer A., Lehnert H., Reitner J. and Worheide G. (2000) Oxygen isotope fractionation in marine aragonite of coralline sponges. *Geochim. Cosmochim. Acta* **64**, 1695–1703.

Cao X. and Liu Y. (2012) Theoretical estimation of the equilibrium distribution of clumped isotopes in nature. *Geochim. Cosmochim. Acta* **77**, 292–303.

Clark I. D. and Lauriol B. (1992) Kinetic enrichment of stable isotopes in cryogenic calcites. *Chem. Geol.* **102**, 217–228.

Craig H., Wharton, Jr., R. A. and McKay C. P. (1992) Oxygen supersaturation in ice-covered Antarctic lakes: biological versus physical contributions. *Science* **255**, 318–321.

Daëron M., Guo W., Eiler J., Genty K., Blamart D., Boch R., Drysdale R. N., Maire R., Wainer K. and Zanchetta G. (2011) ^{13}C–^{18}O clumping in speleothems: observations from natural caves and precipitation experiments. *Geochim. Cosmochim. Acta* **75**, 3303–3317.

Dennis K. J., Affek H. P., Passey B. H., Schrag D. P. and Eiler J. W. (2011) Defining an absolute reference frame for 'clumped' isotope studies of CO_2. *Geochim. Cosmochim. Acta* **75**, 7117–7131.

Dreybrodt W. (1980) Deposition of calcite from thin films on natural calcareous solutions and the growth of speleothems. *Chem. Geol.* **29**, 89–105.

Dreybrodt W. and Scholz D. (2011) Climatic dependence of stable carbon and oxygen isotope signals recorded in speleothems: from soil water to speleothem calcite. *Geochim. Cosmochim. Acta* **75**, 734–752.

Eiler J. M. (2007) "Clumped-isotope" geochemistry – the study of naturally-occurring, multiply-substituted isotopologues. *Earth Planet. Sci. Lett.* **262**, 309–327.

Eiler J. M. (2011) Paleoclimate reconstruction using carbonate clumped isotope thermometry. *Quatern. Sci. Rev.* **30**, 3575–3588.

Fairchild I. J. and Baker A. (2012) *Speleothem Science*. Wiley-Blackwell.

Fairchild I. J., Smith C. L., Baker A., Fuller A., Spötl C., Mattey D., McDermott F. and E.I.M.F. (2006) Modification and preservation of environmental signals in speleothems. *Earth Sci. Rev.* **75**, 105–153.

Ghosh P., Adkins J., Affek H. P., Balta B., Guo W., Schauble E. A., Schrag D. and Eiler J. M. (2006) ^{13}C–^{18}O bonds in carbonate minerals: a new kind of paleothermometer. *Geochim. Cosmochim. Acta* **70**, 1439–1456.

Guo W. (2008) Carbonate clumped isotope thermometry: application to carbonaceous chondrites and effects of kinetic isotope fractionation. Ph. D. thesis, California Institute of Technology, Pasadena, USA.

Haynes, W. M., Lide, D. R. and Bruno, T. J. (eds.) (2012) *CRC Handbook of Chemistry and Physics*, 3rd ed. CRC Press, Taylor and Francis Group, Boca Raton, London, New York.

Hoffmann D. L., Prytulak J., Richards D. A., Elliott T., Coath C. D., Smart P. L. and Scholz D. (2007) Procedures for accurate U and Th isotope measurements by high precision MC-ICPMS. *Int. J. Mass. Spectrom.* **264**, 97–109.

Huntington K. W., Eiler J. M., Affek H. P., Guo W., Bonifacie M., Yeung L. Y., Thiagarajan N., Passey B. H., Tripati A., Daëron M. and Came R. (2009) Methods and limitations of 'clumped' CO_2 isotope (Δ_{47}) analysis by gas-source isotope ratio mass spectrometry. *J. Mass. Spectrom.* **44**, 1318–1329.

IAEA/WMO, 2013. Global network of isotopes in precipitation. The GNIP database. Available on http://isohis.iaea.org, last accessed on July 10, 2013.

Kempe S. (2004) Natural speleothem damage in Postojnska Jama (Slovenia), caused by glacial cave ice? A first assessment. *Acta Cars.* **33**, 265–289.

Killawee J. A., Fairchild I. J., Tison J.-L., Janssens L. and Lorrain R. (1998) Segregation of solutes and gases in experimental freezing of dilute solutions: implications for natural glacial systems. *Geochim. Cosmochim. Acta* **62**, 3637–3655.

Kim S. T. and O'Neil J. R. (1997) Equilibrium and nonequilibrium oxygen isotope effects in synthetic carbonates. *Geochim. Cosmochim. Acta* **61**, 3461–3475.

Kluge T. and Affek H. P. (2012) Quantifying kinetic fractionation in Bunker Cave speleothems using Δ_{47}. *Quatern. Sci. Rev.* **49**, 82–94.

Kluge T., Affek H. P., Marx T., Aeschbach-Hertig W., Riechelmann D. F. C., Scholz D., Riechelmann S., Immenhauser A., Richter C., Fohlmeister J., Wackerbarth A., Mangini A. and Spötl C. (2013) Reconstruction of drip-water $\delta^{18}O$ based on calcite oxygen and clumped isotopes of speleothems from Bunker Cave (Germany). *Clim. Past* **9**, 377–391.

Kunsky J. (1939) Některé formy ledovych krápníků. Rozpravy I. *I. Třídy České akademie* **49**, 1–8.

Lacelle D. (2007) Environmental setting, (micro)morphologies and stable C–O isotope composition of cold climate carbonate precipitates; a review and evaluation of their potential as paleoclimatic proxies. *Quatern. Sci. Rev.* **26**, 1670–1689.

Lacelle D., Lauriol B. and Clark I. D. (2009) Formation of seasonal ice bodies and associated cryogenic carbonates in Caverne de l'Ours, Québec, Canada: kinetic isotope effects and pseudo-biogenic crystal structures. *J. Cave Karst Stud.* **71**, 48–62.

Lachniet M. S. (2009) Climatic and environmental controls on speleothem oxygen isotope values. *Quatern. Sci. Rev.* **28**, 412–432.

Lehmann M. and Siegenthaler U. (1991) Equilibrium oxygen- and hydrogen-isotope fractionation between ice and water. *J. Glaciol.* **37**, 23–26.

Luetscher M., Borreguero M., Moseley G. E., Spötl C. and Edwards R. L. (2013) Alpine permafrost thawing during the Medieval Warm Period identified from cryogenic cave carbonates. *Cryosphere* **7**, 1073–1081.

McDermott F. (2004) Palaeo-climate reconstruction from stable isotope variations in speleothems: a review. *Quatern. Sci. Rev.* **23**, 908–918.

McDermott F., Atkinson T. C., Fairchild I. J., Baldini L. M. and Mattey D. P. (2011) A first evaluation of the spatial gradients in $\delta^{18}O$ recorded by European Holocene speleothems. *Global Planet. Change* **79**, 275–287.

Mickler P. J., Stern L. A. and Banner J. L. (2006) Large kinetic isotope effects in modern speleothems. *GSA Bull.* **118**, 65–81.

Mook W. G. (2000) Environmental isotopes in the hydrological cycle: principles and applications. In *Introduction, Theory, Methods, Review. IHP-V: Technical Documents in Hydrology, vol. 1* (ed. W. G. Mook). No. 39, UNESCO, Paris.

Mook W. G., Bommerson J. C. and Staverman W. H. (1974) Carbon isotope fractionation between dissolved bicarbonate and gaseous carbon dioxide. *Earth Planet. Sci. Lett.* **22**, 169–176.

Mühlinghaus C., Scholz D. and Mangini A. (2009) Modelling fractionation of stable isotopes in stalagmites. *Geochim. Comochim. Acta* **73**, 7275–7289.

Namiot A. Y. and Bukhgalter E. B. (1965) Clathrates formed by gases in ice. *J. Struct. Chem.* **6**, 873–874.

O'Neil J. R. (1968) Hydrogen and oxygen isotope fractionation between ice and water. *J. Phys. Chem.* **72**, 3683–3684.

Pieitkäinen J., Pettersson M. and Bååth E. (2005) Comparison of temperature effects on soil respiration and bacterial and fungal growth rates. *FEMS Microbiol. Ecol.* **52**, 49–58.

Pielsticker K.-H. (2000) Höhlen und Permafrost – Thermophysikalische Prozesse von Höhlenvereisungen während des Quartärs. *Bochumer Geol. Geotech. Arbeit.* **55**, 187–196 (in German).

Renssen H. and Vandenberghe J. (2003) Investigation of the relationship between permafrost distribution in NW Europe and extensive winter sea-ice cover in the North Atlantic Ocean during the cold phases of the Last Glaciation. *Quatern. Sci. Rev.* **22**, 209–223.

Richter D. K. and Riechelmann D. F. C. (2008) Late Pleistocene cryogenic calcite spherolites from the Malachitdom Cave (NE Rhenish Slate Mountains, Germany): origin, unusual internal structure and stable C–O isotope composition. *Int. J. Speleol.* **37**, 119–129.

Richter D. K., Neuser R. D. and Voigt S. (2008) Cryogenic calcite particles from the Heilenbecker Cave in Ennepetal (NE Bergisches Land/North-Rhine Westphalia). *Die Höhle* **59**, 24–34 (in German, abstract in English).

Richter D. K., Mangini A. and Voigt S. (2009) Erste Th/U-datierte Kryocalcite der mittleren Weichseleiszeit aus einer Höhle des Rheinischen Schiefergebirges (Heilenbecker Höhle, Bergisches Land). *Mitt. Verb. Deutsch. Höhlen. u. Karstforsch.* **55**, 125–127 (in German, abstract in English).

Richter D. K., Meissner P., Immenhauser A., Schulte U. and Dorsten I. (2010) Cryogenic and non-cryogenic pool calcites indicating permafrost and non-permafrost periods: a case study from the Herbstlabyrinth-Advent Cave system (Germany). *Cryosphere* **4**, 501–509.

Richter D. K., Mischel S., Dorsten I., Mangini A., Neuser R. D. and Immenhauser A. (2011) Zerbrochene Höhlensinter und Kryocalcite als Indikatoren für eiszeitlichen Permafrost im Herbstlabyrinth-Adventhöhle-System bei Breitscheid-Erdbach (N-Hessen). *Die Höhle* **62**, 31–45 (in German, abstract in English).

Richter D. K., Meyer S., Scholz D. and Immenhauser A. (2013) Multiphase formation of Weichselian cryogenic calcites, Riesenberg Cave NW Germany. *German J. Geosci.* **164**, 353–367.

Riechelmann D. F. C., Schröder-Ritzrau A., Scholz D., Fohlmeister J., Spötl C., Richter D. K. and Mangini A. (2011) Monitoring Bunker Cave (NW Germany): a prerequisite to interpret geochemical proxy data of speleothems from this site. *J. Hydrol.* **409**, 682–695.

Scholz D. and Hoffmann D. (2008) ^{230}Th/U dating of fossil corals and speleothems. *Eiszeit. Gegenw.* **57**, 52–76.

Scholz D., Mühlinghaus C. and Mangini A. (2009) Modelling $\delta^{13}C$ and $\delta^{18}O$ in the solution layer on stalagmite surfaces. *Geochim. Cosmochim. Acta* **73**, 2592–2602.

Spötl C. (2008) Kryogene Karbonate im Höhleneis der Eisriesenwelt. *Die Höhle* **59**, 26–36 (in German, abstract in English).

Tremaine D. M., Froelich P. N. and Wang Y. (2011) Speleothem calcite farmed in situ: modern calibration of $\delta^{18}O$ and $\delta^{13}C$ paleoclimate proxies in a continuously-monitored natural cave system. *Geochim. Cosmochim. Acta* **75**, 4929–4950.

Vaikmäe R., Edmunds W. M., and Manzano M. (2001) Weichselian palaeoclimate and palaeoenvironment in Europe: background for palaeogroundwater formation. In *Palaeowaters in Coastal Europe: Evolution of Groundwater Since the Late Pleistocene* (eds. W. M. Edmunds and C. J. Milne). Geological Society, London, Special Publications. 189, pp. 163–191.

Van Vliet-Lanoë B. (1989) Dynamics and extent of the Weichselian permafrost in western Europe (substage 5e to stage 1). *Quatern. Int.* **3–4**, 109–113.

Vandenberghe J., Renssen H., Roche D. M., Goose H., Velichko A. A., Gorbunov A. and Levavasseur G. (2012) Eurasian permafrost instability constrained by reduced sea-ice cover. *Quatern. Sci. Rev.* **34**, 16–23.

von Grafenstein U., Erlenkeuser H., Brauer A., Jouzel J. and Johnsen S. J. (1999) A mid-European decadal isotope-climate record from 15,500 to 5000 years B.P. *Science* **284**, 1654–1657.

Wainer K., Genty D., Blamart D., Daëron M., Bar-Matthews M., Vonhof H., Dublyansky Y., Pons-Branchu E., Thomas L., van Calsteren P., Quinif Y. and Caillon N. (2011) Speleothem record of the last 180 ka in Villars cave (SW France): Investigation of a large $\delta^{18}O$ shift between MIS6 and MIS5. *Quatern. Sci. Rev.* **30**, 130–146.

Wang Z., Schauble E. A. and Eiler J. M. (2004) Equilibrium thermodynamics of multiply substituted isotopologues of molecular gases. *Geochim. Cosmochim. Acta* **68**, 4779–4797.

Wiedner E., Scholz D., Mangini A., Polag D., Mühlinghaus C. and Segl M. (2008) Investigation of the stable isotope fractionation in speleothems with laboratory experiments. *Quatern. Int.* **187**, 15–24.

Zaarur S., Olack G. and Affek H. P. (2011) Paleo-environmental implication of clumped isotopes in land snail shells. *Geochim. Cosmochim. Acta* **75**, 6859–6869.

Zaarur S., Affek H. P. and Brandon M. T. (2013) A revised calibration of the clumped isotope thermometer. *Earth Planet. Sci. Lett.* **382**, 47–57.

Žák K., Urban J., Cilek V. and Hercman H. (2004) Cryogenic cave calcite from several Central European caves; age, carbon and oxygen isotopes and a genetic model. *Chem. Geol.* **206**, 119–136.

Žák K., Onac B. P. and Perşoiu A. (2008) Cryogenic carbonates in cave environments: a review. *Quatern. Int.* **187**, 84–96.

Žák K., Richter D. K., Filippi M., Živor R., Deininger M., Mangini A. and Scholz D. (2012) Coarsely crystalline cryogenic cave carbonate – a new archive to estimate the Last Glacial permafrost depth in Central Europe. *Clim. Past* **8**, 1821–1837.

Associate editor: Miryam Bar-Matthews